ECS Journal of Solid State
Science and Technology

OPEN ACCESS

Influence of Oxygen Pressure on Growth of Si-Doped β-$(Al_xGa_{1-x})_2O_3$ Thin Films on c-Sapphire Substrates by Pulsed Laser Deposition

To cite this article: A. Hassa *et al* 2019 *ECS J. Solid State Sci. Technol.* **8** Q3217

JSS Focus Issue on Gallium Oxide Based Materials and Devices

Influence of Oxygen Pressure on Growth of Si-Doped β-$(Al_xGa_{1-x})_2O_3$ Thin Films on c-Sapphire Substrates by Pulsed Laser Deposition

A. Hassa,[1,z] **H. von Wenckstern,**[1] **L. Vines,**[2] **and M. Grundmann**[1]

[1] *Felix Bloch Institute for Solid State Physics, Universität Leipzig, Sachsen 04103, Germany*
[2] *Department of Physics, Centre for Materials Science and Nanotechnology, University of Oslo, Oslo 0316, Norway*

Ga_2O_3 is a deep-UV transparent semiconducting oxide being interesting for solar-blind photo detectors e.g. for flame or missile plume detection. The bandgap of about 4.9 eV can be increased by alloying with Al_2O_3. We have investigated β-$(Al,Ga)_2O_3$ thin films grown by pulsed laser deposition (PLD) on (00.1) Al_2O_3 with regard to the influence of the growth parameters such as growth temperature (T_g) and oxygen partial pressure ($p(O_2)$) on the structural, optical and electrical properties of the samples. The thin films have (-201) orientation and the cation incorporation strongly depends on the deposition parameters. At a given T_g, the incorporation of Al is favored for lower $p(O_2)$ due to higher dissociation energy of the Al-O bond compared to the Ga-O bond. At a given $p(O_2)$, the incorporation of Al is favored for higher T_g due to desorption of gallium sub-oxides during growth.
 [DOI: 10.1149/2.0411907jss]

Manuscript submitted January 16, 2019; revised manuscript received April 5, 2019. Published April 24, 2019. *This paper is part of the JSS Focus Issue on Gallium Oxide Based Materials and Devices.*

The wide bandgap semiconductor gallium oxide is more and more explored for high-power electronics, because of its promising material properties, such as beneficial breakdown voltages and large power semiconductor device figures of merit. Further applications include quantum well infrared photodetectors or deep UV-photodetectors like flame sensors for missile plume detection, biological and chemical sensors for ozone detection or gas sensors. In addition, Ga_2O_3 finds use in touch panel displays, solar cells or optical communications, such as intra- and inter-satellite secured communication systems.[1–3]

Ga_2O_3 occurs in different polymorphs, denoted by α, β, γ, δ, ϵ,[4] and κ.[5] Because of it is thermodynamical stability, the monoclinic β-structure is the most studied phase, so far. The large bandgap energy of the binary oxide ranges between 4.7 and 5.0 eV. The optical anisotropy and dichroism have been investigated in detail in Ref. 6. The gap can be tuned by alloying with In_2O_3 or Al_2O_3.[1–3] Up to now conducting $(In,Ga)_2O_3$ thin films with a tailored bandgap could be produced and devices based on the ternary alloy were realized.[2,7] The most challenging part will be the fabrication of conducting $(Al,Ga)_2O_3$ thin films. Since intrinsic defects such as oxygen vacancies do not contribute to the conduction of Ga_2O_3,[8] extrinsic doping is necessary to realize electrical devices.[9] Possible suitable cations for doping are silicon,[2,10–12] tin[2,13] or germanium[2,14] Hence these cations are part of the present study to create conducting samples. In the β-Ga_2O_3 crystal structure, Al replaces Ga at octahedral sites, which induces changes of the crystal structure and thereby in the lattice constants as reported by Kranert et al.[15] Schmidt-Grund et al. investigated the relating bandgap dependency on the aluminum content x_{Al}, which can be described by the formula $E_g = (4.811 + 2.138\, x_{Al})$ eV for $0.11 \leq x_{Al} \leq 0.55$.[16]

In the fabrication of thin films by means of pulsed laser deposition (PLD) the oxygen pressure $p(O_2)$ and growth temperature T_g influence the growth process and the thin film properties independently. For binary β-Ga_2O_3 thin films, Müller et al. observed decreasing growth rates with decreasing $p(O_2)$[12] and Zha et al. reported decreasing growth rates with increasing T_g.[17] For ternary $(Al,Ga)_2O_3$ thin films, Wang et al. characterized the influence of the growth temperature and showed that for increasing T_g lower growth rates were observed.[18] Wakabayashi et al. showed the influence of $p(O_2)$ on PLD grown $(Al,Ga)_2O_3$ samples.[19] For low oxygen pressures they observed a decrease of the growth rate and a non-stoichiometric transfer of Ga and Al atoms. They showed that this process can be suppressed by using an oxygen-radical atmosphere during growth. As a result the growth rates recovered and a stoichiometric transfer was observed.[19] Further, Feng et al. reported a non-stoichiometric cation transfer from target to sample for PLD grown $(Al,Ga)_2O_3$ thin films, which was attributed to the formation of the volatile suboxide Ga_2O.[20] The choice of oxygen pressure and/or growth temperature during PLD influence the growth rate and cation composition of $(Al,Ga)_2O_3$. Therefore, it is of great importance to understand the growth process and the formation of volatile gallium suboxides as a function of $p(O_2)$ and T_g. The central aspect of this work is the determination of the growth window for which stoichiometric cation incorporation occurs. Furthermore, it summarizes our attempts to fabricate electrically conducting thin films.

Experimental

The samples investigated in this study were grown by pulsed laser deposition (PLD) on (00.1) Al_2O_3. The ceramic targets for PLD consist of Ga_2O_3 with 8.8 at.% Al_2O_3 and were additionally doped with different amounts of tin, silicon or germanium to improve electrical conductivity. The growth temperature and growth pressure were changed in a wide parameter space as can be seen in Table I. For the ablation we used a KrF excimer laser (248 nm) with an energy density of 2 Jcm^{-2} at the target and a frequency of 15 Hz. The target to substrate distance was 10 cm. The number of laser pulses was 30300 and the resulting film thicknesses ranges between 400 and 1200 nm. Moreover, series of samples were implanted with tin or silicon using a 1 MeV Tandem accelerator from NEC. For each sample different implantation energies, for Si, 36, 160 and 600 keV and with fluencies of 1.5×10^{13}, 6×10^{13}, and 1.5×10^{14} cm^{-2}, respectively, were used to obtain a homogeneous implantation profile. For the Sn implanted samples we applied 600 keV

Table I. Range of Growth temperature T_g, oxygen partial pressure $p(O_2)$ and cation composition of the used PLD targets.

Target: Ga_2O_3 + 8.8 at.% Al_2O_3 +	Growth parameters: T_g in °C	$p(O_2)$ in mbar
0.2–4.4 at% SiO_2	490–670	3×10^{-4}–0.04
0.6 at% SnO_2	400–670	3×10^{-4}–0.024
0.9–4 at% GeO_2	420–670	3×10^{-4}–0.02

[z]E-mail: anna.hassa@physik.uni-leipzig.de

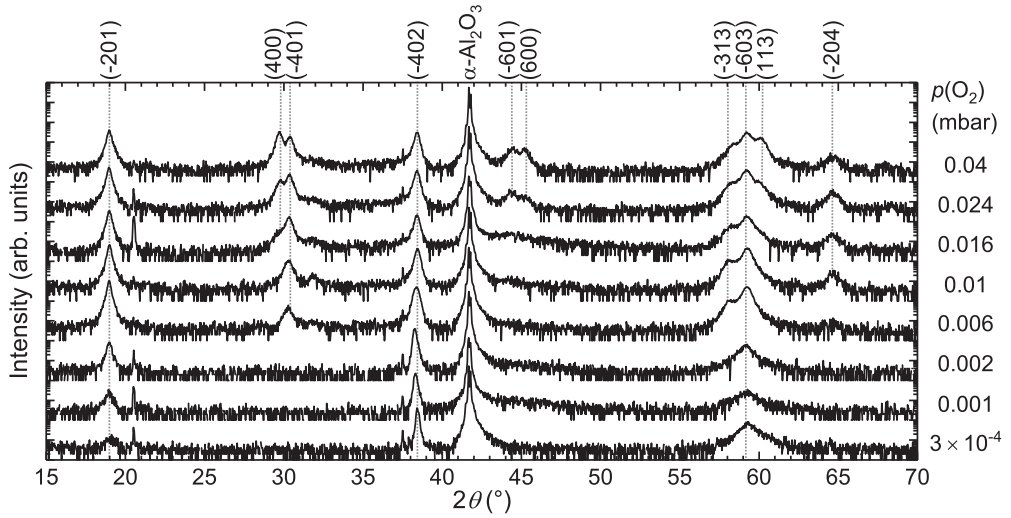

Figure 1. XRD 2θ-ω scans of $(Al,Ga)_2O_3$:Si thin films deposited at a growth temperature of 670°C and different oxygen partial pressures as labeled. The peaks were assigned to reflections at lattice planes as labeled by comparison with JCPDS Card #76-0573.

and 2 MeV and with doses of 5×10^{13} and 1×10^{14} cm^{-2}. To activate the implanted Si and Sn, the samples were annealed at approximately 840°C for one hour in nitrogen ambient. Thin film properties as the alloy composition, structural, optical and electrical properties were investigated by means of energy-dispersive X-ray spectroscopy (EDX), X-ray diffraction (XRD), atomic force microscopy (AFM), and Hall effect measurements. The respective bandgap energies E_g and layer thicknesses d were determined by transmission measurements. By extrapolation of $(\alpha h\nu)^2$ vs. photon energy to zero the bandgap energies were estimated and d can be calculated from observable layer thickness oscillations using a refractive index of $n \approx 2$.[21] There, α describes the absorption coefficient, h the Planck constant and ν the wave frequency. For the transport measurements, ohmic contacts, consisting of 30 nm thick layers of titanium, aluminum and gold (Ti/Al/Au), respectively, were thermally evaporated on the corners of the square samples through a shadow mask. Subsequently, these contacts were annealed at 500°C for 10 minutes in a nitrogen ambient.

Results and Discussion

The influence of the oxygen pressure during growth will be discussed in the following section based on a growth series deposited at a growth temperature of 670°C. The used target consists of 86.8 at.% Ga_2O_3 + 8.8 at.% Al_2O_3 + 4.4 at.% SiO_2 and the oxygen pressure was varied in the range from 0.04 to 3×10^{-4} mbar. XRD patterns, shown in Figure 1, indicate a strong influence of $p(O_2)$ on the crystallinity of the samples. The peak appearing at $2\theta = 41.68°$ can be assigned to reflections on the (00.6) plane of the c-plane sapphire substrate. The remaining visible reflection peaks belong to monoclinic gallium oxide. For Ga_2O_3. For $p(O_2) \leq 0.002$ mbar the thin films grow only in [-201]-direction and show reflection peaks at 2θ angles of 18.9°, 38.4° and 59.2° corresponding to reflections at the (-201) lattice planes. Zhang et al. and Wang et al. already reported that β-$(Al,Ga)_2O_3$ thin films on sapphire substrates grow in [-201]-direction [18,22] as it is the case for binary Ga_2O_3.[2] Nakagomi and Kokubun recognized, that the order of oxygen atoms of the (001) plane of c-sapphire and the corresponding (-201) plane of β-Ga_2O_3 is equal[23] leading to a minor mismatch between both lattice planes. For growth pressure between 0.006 and 0.016 mbar additionally peaks at 30.4°, 58.3° and 64.7° occur and correspond to reflections at the (-401)-, (-313)- and (-204)-planes, respectively. Further reflection peaks at $2\theta = 29.8°$, 44.2°, 45.3°, and 60° are visible for $p(O_2) = 0.024$ - 0.04 mbar and corresponds to the (400)-, (-601)-, (600)-, and (113)-planes.

As the oxygen pressure in the PLD chamber increases, the kinetic energy of the atomic and molecular species arriving at the substrate decreases. The resulting smaller diffusion length leads to the formation of smaller grains, increasing the probability that some of these grains grow in an orientation different from (-201). This effect is in contrast to many other oxide film systems crystallizing in the higher symmetry cubic or hexagonal structure.[24] The correlation of oxygen pressure and crystal growth was reported by Müller et al., who observed for binary Ga_2O_3 similar behavior.[12]

Figure 2a shows the calculated growth rates (r = d/#pulses), bandgap energies and aluminum content from the $(Al_xGa_{1-x})_2O_3$:SiO_2 growth series and its dependence on the growth pressure. The bandgap

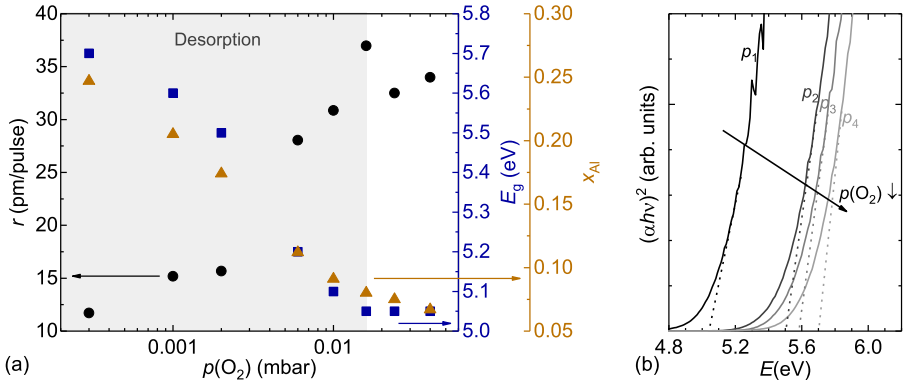

Figure 2. (a) Measured growth rate r, bandgap E_g and aluminum concentration x_{Al} in dependence on the logarithmic oxygen partial pressure $p(O_2)$. The gray shaded area indicates the $p(O_2)$ regime where desorption is essential. (b) Optical transmittance spectra for oxygen pressures of $p_1 = 0.04$ mbar, $p_2 = 0.002$ mbar, $p_3 = 0.001$ mbar, and $p_4 = 3 \times 10^{-4}$ mbar.

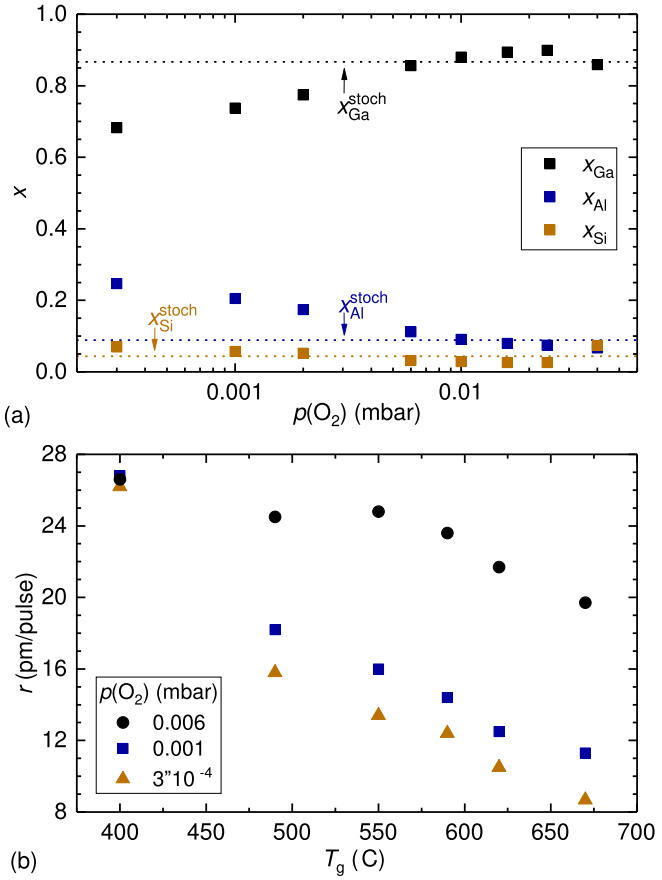

Figure 3. (a) Cation concentration of gallium, aluminum and silicon atoms measured by EDX in dependence of the growth pressure deposited at a growth temperature of 670°C. The dotted lines indicate elemental concentration for a stoichiometric transfer of the target composition being $x_{Ga}^{stoch} = 0.868$, $x_{Al}^{stoch} = 0.088$ and $x_{Si}^{stoch} = 0.044$. (b) Dependency of the growth rate on the growth temperature for three chosen oxygen pressures as labeled in the picture.

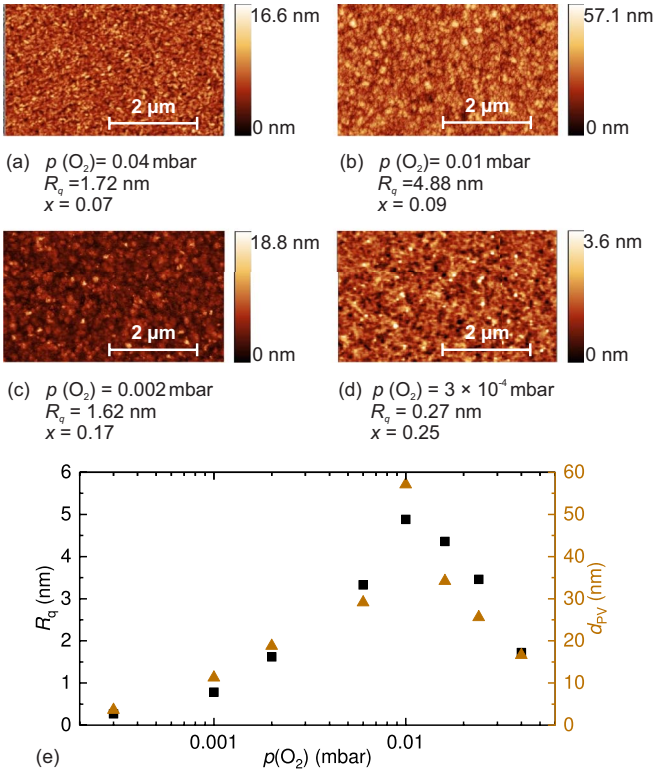

Figure 4. R_q describes the mean square roughness and x the aluminum content. The scale next to the pictures (a) to (d) characterizes the peak-valley-distance (d_{PV}). The thin films are deposited at $T_g = 670$°C and different oxygen partial pressures as labeled. (e) shows the dependency of R_q and d_{PV} to the oxygen pressure.

energies were calculated from the optical transmittance spectra and are shown for four different oxygen pressures in Fig. 2b. In Fig. 2a a division into two growth regimes ($p(O_2) \geq 0.016$ mbar and $p(O_2) < 0.016$ mbar) is recognizable. For $p(O_2) \geq 0.016$ mbar similar growth rates of 32.5 to 37 pm/pulse, bandgap energies of approximately 5.05 eV and an aluminum content ranging between 0.06 and 0.08 were observed, as well. Below an oxygen pressure of 0.016 mbar the growth rate decreases with decreasing growth pressure up to a value of 12 pm/pulse for 3×10^{-4} mbar. Simultaneously, the bandgap energies and aluminum contents increases up to values of $E_g = 5.7$ eV and $x_{Al} = 0.25$. The influence of the oxygen pressure on the cation composition is illustrated in Figure 3a and show, that with decreasing growth pressure the gallium (aluminum) content x_{Ga} (x_{Al}) decreases (increases) for a given growth temperature of 670°C. The sum of all incorporated cations is always 1 and the silicon proportion ranges between 0.03 and 0.07.

For oxygen pressures between 0.04 and 0.016 mbar a nearly stochiometric transfer of the Ga, Al and Si atoms from target to layer is observed and results in similar growth rates and bandgaps (see Fig. 2). In the oxygen regime below 0.016 mbar, aluminum atoms are preferentially incorporated, because of the higher dissociation energy of the Al-O bond compared to the Ga-O bond.[25] Further, gallium forms volatile sub-oxides being desorbed. As a result, considerably lower amounts of Ga are incorporated into the layers as seen in Figure 3a. The higher aluminum content leads to the observed bandgap increase and the desorption of gallium sub-oxides leads to lower growth rates. Similar desorption processes were reported for molecular beam epitaxy growth of In_2O_3, Ga_2O_3 and $(In_xGa_{1-x})_2O_3$ thin films by Vogt and Bierwagen.[26–28] Since the desorption is a temperature dependent process, we investigated the growth rates of samples deposited at three different oxygen pressures (0.006, 0.001 and 3×10^{-4} mbar) and various growth temperatures (from 400 to 670°C). For deposition of these sample series we used a target consisting of Ga_2O_3 + 8.8 at.% Al_2O_3 + 0.6 at.% SnO_2. The growth rates, depicted in Figure 3b, decreases with increasing temperature showing that the formation of volatile suboxides is favorable at higher growth temperatures. For the highest investigated oxygen pressure of 0.006 mbar saturation of the growth rate with values between 24.5 to 26.2 pm/pulse is observed for growth temperatures below 550°C.

Using AFM on areas of $3 \times 5\,\mu m^2$ the surface morphology and consequently the root mean square surface roughness R_q and peak-valley-distance d_{PV} were examined. Figure 4 displays the R_q and d_{PV} values obtained from the already discussed $(Al_xGa_{1-x})_2O_3$:SiO_2 growth series. The visible surface effects can be divided into two categories for $p(O_2) < 0.01$ mbar and $p(O_2) \geq 0.01$ mbar. For oxygen pressures below 0.01 mbar R_q and d_{PV} depend on the aluminum content. With increasing x_{Al} the surface becomes smoother and the roughness decreases from $R_q = 3.33$ nm for $x_{Al} = 0.11$ to $R_q = 0.27$ nm for $x_{Al} = 0.25$. For $p(O_2) \geq 0.01$ mbar the aluminum content saturates and hence the oxygen pressure is determining the surface morphology. The surface roughness increases from $R_q = 1.72$ nm for 0.04 mbar to $R_q = 4.88$ nm for 0.01 mbar.

Currently, the most challenging task for the growth of ternary heteroepitaxial $(Al,Ga)_2O_3$ thin films is the development of a doping strategy in order to tailor its electrical transport properties. As part of this work various tests were executed to obtain conducting thin films. All samples investigated were electrically insulating. Concerning the doping of the thin films, we doped samples during growth process in situ and additionally we used ion implantation to create

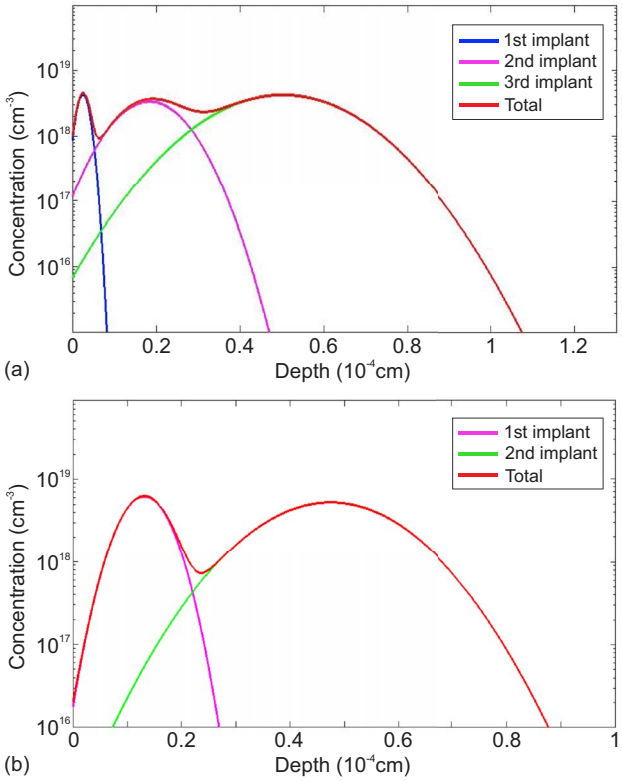

Figure 5. Implantation profile of (a) Si and (b) Sn.

conducting samples, ex situ. For the implantation process a nearly homogeneous dopant concentration of approximately (1–5) $\times 10^{18}$ cm^{-3} was realized for both, Si and Sn, as visible in Fig. 5. Before and after annealing, however, all samples remained insulating as soon as Al was alloyed.

Conclusions

We have discussed the influence of growth conditions on the crystallinity, bandgap energy, growth rate, cation composition and surface morphology of PLD-grown $(Al,Ga)_2O_3$ thin films on c-sapphire substrates. We described that the preferential incorporation of Al was in tendency observed for low oxygen pressures and/or high growth temperature, which was assigned to differences in cation oxygen bond strength and desorption of gallium sub oxide. Decreasing growth pressure lead to decreasing growth rates and low gallium content. Lower growth temperatures favor the stoichiometric cation incorporation into the thin film layer. Further, many different growth conditions were pointed out to produce insulating samples. It can be concluded that it was not possible to produce conductive samples. This issue must be solved prior to the fabrication of devices based on $(Al,Ga)_2O_3$.

Acknowledgments

We thank Monika Hahn for PLD target fabrication, Jörg Lenzner for EDX, and Ulrike Teschner for transmission measurements. This work was supported by European Social Fund within the Young Investigator Group "Oxide Heterostructures" (SAB 100310460) and partly by Deutsche Forschungsgemeinschaft in the Framework of Sonderforschungsbereich 762 "Functionality of Oxide Interfaces". A.H. acknowledges the Leipzig School for Natural Sciences BuildMoNa.

ORCID

A. Hassa https://orcid.org/0000-0002-8087-6592
H. von Wenckstern https://orcid.org/0000-0002-3936-275X
L. Vines https://orcid.org/0000-0001-5759-7192
M. Grundmann https://orcid.org/0000-0001-7554-182X

References

1. S. I. Stepanov, V. I. Nikolaev, V. E. Bougrov, and A. Romanov, *Reviews on Advanced Materials Science*, **44**, 63 (2016).
2. H. von Wenckstern, *Advanced Electronic Materials*, **3**, 1600350 (2017).
3. S. J. Pearton, J. Yang, P. H. Cary, F. Ren, J. Kim, M. J. Tadjer, and M. A. Mastro, *Applied Physics Reviews*, **5**, 011301 (2018).
4. R. Roy, V. G. Hill, and E. F. Osborn, *Journal of the American Chemical Society*, **74**, 719 (1952).
5. H. Y. Playford, A. C. Hannon, E. R. Barney, and R. I. Walton, *Chemistry - A European Journal*, **19**, 2803 (2013).
6. C. Sturm, J. Furthmüller, F. Bechstedt, R. Schmidt-Grund, and M. Grundmann, *APL Materials*, **3**, 106106 (2015).
7. S. J. Pearton, M. A. Mastro, and F. Ren, *Elsevier* (2018).
8. L. Dong, R. Jia, B. Xin, B. Peng, and Y. Zhang, *Scientific Reports*, **7**, 40160 (2017).
9. J. B. Varley, J. R. Weber, A. Janotti, and C. G. Van de Walle, *Applied Physics Letters*, **97**, 142106 (2010).
10. E. G. Víllora, K. Shimamura, Y. Yoshikawa, T. Ujiie, and K. Aoki, *Applied Physics Letters*, **92**, 202120 (2008).
11. D. Splith, S. Müller, F. Schmidt, H. von Wenckstern, J. J. van Rensburg, W. E. Meyer, and M. Grundmann, *Physica Status Solidi (a)*, **211**, 40 (2014).
12. S. Müller, H. von Wenckstern, D. Splith, F. Schmidt, and M. Grundmann, *Physica Status Solidi (a)*, **211**, 34 (2014).
13. N. Suzuki, S. Ohira, M. Tanaka, T. Sugawara, K. Nakajima, and T. Shishido, *Physica Status Solidi (c)*, **4**, 2310 (2007).
14. E. Ahmadi, O. S. Koksaldi, X. Zheng, T. Mates, Y. Oshima, U. K. Mishra, and J. S. Speck, *Applied Physics Express*, **10**, 071101 (2017).
15. C. Kranert, M. Jenderka, J. Lenzner, M. Lorenz, H. von Wenckstern, R. Schmidt-Grund, and M. Grundmann, *Journal of Applied Physics*, **117**, 125703 (2015).
16. R. Schmidt-Grund, C. Kranert, H. von Wenckstern, V. Zviagin, M. Lorenz, and M. Grundmann, *Journal of Applied Physics*, **117**, 165307 (2015).
17. F. Zhang, K. Saito, T. Tanaka, M. Nishio, and Q. Guo, *Journal of Crystal Growth*, **387**, 96 (2014).
18. X. Wang, Z. Chen, F. Zhang, K. Saito, T. Tanaka, M. Nishio, and Q. Guo, *Ceramics International*, **42**, 12783 (2016).
19. R. Wakabayashi, T. Oshima, M. Hattori, K. Sasaki, T. Masui, A. Kuramata, S. Yamakoshi, K. Yoshimatsu, and A. Ohtomo, *Journal of Crystal Growth*, **424**, 77 (2015).
20. Q. Feng, Z. Hu, Z. Feng, X. Xing, Y. Zuo, G. Yan, X. Lu, C. Zhang, H. Zhou, and J. Zhang, *Superlattices and Microstructures*, **120**, 441 (2018).
21. A. Petitmangin, C. Hébert, J. Perrière, B. Gallas, L. Binet, P. Barboux, and P. Vermaut, *Journal of Applied Physics*, **109**, 013711 (2011).
22. F. Zhang, K. Saito, T. Tanaka, M. Nishio, M. Arita, and Q. Guo, *Applied Physics Letters*, **105**, 162107 (2014).
23. S. Nakagomi and Y. Kokubun, *Journal of Crystal Growth*, **349**, 12 (2012).
24. M. Lorenz, *Encyclopedia of Applied Physics*, Wiley-VCH Verlag GmbH & Co. KGaA (Ed.), (2019).
25. Y.-R. Luo, *Comprehensive Handbook of Chemical Bond Energies*, CRC Press (2007).
26. P. Vogt and O. Bierwagen, *Applied Physics Letters*, **106**, 081910 (2015).
27. P. Vogt and O. Bierwagen, *APL Materials*, **4**, 086112 (2016).
28. P. Vogt and O. Bierwagen, *Applied Physics Letters*, **108**, 072101 (2016).